Solar Energy Materials & Solar Cells 147 (2016) 157–163

Contents lists available at ScienceDirect

Solar Energy Materials & Solar Cells

journal homepage: www.elsevier.com/locate/solmat

Robust surface passivation of trap sites in PbS q-dots by controlling the thickness of CdS layers in PbS/CdS quantum dot solar cells

Arumukham Manjceevan, Jayasundera Bandara *

Institute of Fundamental Studies, Hantana Road, Kandy, CP 20000, Sri Lanka

ARTICLE INFO

Article history:
Received 28 September 2015
Received in revised form
10 December 2015
Accepted 13 December 2015

Keywords:
Sensitized solar cells
Quantum dots
Lead sulfide
Cadmium sulfide
Passivation effects

ABSTRACT

The PbS quantum dot sensitized solar cells were prepared on 3-mercaptoproponic acid (MPA) anchored mesoporous TiO_2 films by a successive ionic layer adsorption and reaction (SILAR) process and the fabricated PbS q-dots were passivated by deposition of a CdS layer. In SILAR process, MPA solution was mixed with sulfide precursor solution and used it in every SILAR cycle for rapid conversion of Pb and Cd into their respective sulfides form. Performances of surface passivated and non-passivated PbS q-dot solar cells were compared where solar cells fabricated with q-dots of PbS, PbS/CdS, CdS showed best efficiencies (η) of 1.0, 5.7, 0.9% with current densities (Jsc) of 10.1, 22.8, 2.7 mA cm^{-2} and open circuit voltages (Voc) of 280, 501, 498 mV respectively. The enhanced efficiency of PbS/CdS q-dot solar cell was mainly due to increase in Jsc and Voc compared to PbS q-dot solar cells. The outstanding performance of PbS/CdS sensitized solar cell was found to be due to reduction of trap states in PbS particle by the surface passivation effect of CdS q-dots and the surface passivation effect of CdS in PbS/CdS sensitized solar cell is reported by EIS and voltage decay investigations.

1. Introduction

Inorganic semiconductors are promising as light harvesting material for next generation q-dot sensitized solar cells [1]. Attractive feature of q-dots is the ability to tune the band gap of q-dots to harvest near infra-red to ultraviolet region of the solar spectrum [2]. Characteristic features of q-dots such as tunable band gaps and broad-band absorption properties, persuade scientific research interest on semiconductor sensitized solar cells [3]. Light harvesting q-dots can be anchored on high bandgap mesoporous semiconductor materials to sensitize the semiconductor based photoanode resembling to configuration of dye sensitized solar cells (DSSC) [4]. In recent investigations, 8 and 7.5% solar cell efficiencies were reported for q-dot solar cells fabricated with PbS [5] and Sb_2S_3 [6] respectively, yet these efficiencies are inferior to that of DSSC.

Co-sensitized PbS/CdS q-dot solar cells are found to be the promising choice in q-dot solar cells due to their efficient light harvesting properties, ease of fabrication and the low cost. By using SILAR method, PbS/CdS has been anchored on TiO_2, ZnO, SnO_2 and achieved 2.3% efficiency with SnO_2 photoelectrode [7]. In a recent investigation, 4% efficiency has been reported for PbS/TiO_2 photoelectrode by anchoring PbS on TiO_2 photoanode by SILAR method [8]. In the same investigation, the effect of precursor solution on the performance of solar cell was investigated and reported that lead acetate performed better than lead nitrate precursor due to higher loading of q-dots on mesoporous layer by using lead acetate precursor solution. A further enhancement of efficiency of PbS/CdS q-dot solar cells has been reported by passivation of q-dot by passivating agents such as dimethylamine, formic acid, ethanedithiol and thioglycolic acid and the highest efficiency of 4.65% was reported with ethanedithiol passivating agent which was found to be the highest recorded efficiency for PbS/CdS quantum dot solar cell [9]. The major problems in PbS/CdS q-dot sensitized solar cells are rapid charge recombination due to presence of trap sites in PbS particles and poor stability due to spontaneous oxidation by thermally activation [10] and electrochemical corrosion [11,12].

In PbS/CdS solar cell structures, CdS has been employed mainly as complementary light harvesting species [13]. To minimize the inherent charge recombination properties of PbS/CdS anode, passivating agents have been used [9]. However, in this investigation, we demonstrated that CdS layer on PbS could also function as a surface passivation layer for PbS q-dot particles and reduce the charge recombination centers in PbS particles. We used combined SILAR method with bidentate linker molecule to achieve higher loading of q-dot PbS on mesoporous TiO_2 photoanode and q-dot CdS on PbS layers. The SILAR method is found to be the easiest and cheapest method to fabricate the q-dot solar cells by varying the number of deposition cycle [7,14] and concentrations of solutions

* Corresponding author.
E-mail addresses: bandaraj@ifs.ac.lk, jayasundera@yahoo.com (J. Bandara).

http://dx.doi.org/10.1016/j.solmat.2015.12.014
0927-0248/

[8,15] with capability of controlling the quantum confinement effect. The effect of loading of PbS as well as CdS on solar cell performance specially on short circuit current density (Jsc), open circuit voltage (Voc), fill factor (FF) and the overall solar cell efficiency (η) were investigated. Furthermore, the function of PbS and CdS layers on light harvesting as well as passivation were also investigated.

2. Experimental section

2.1. Materials and fabrication

Titanium(IV)isopropoxide (97%, Fluka), ethylene glycol (99.9%, AnalR Normapur), citric acid (99.5%, Avondale Laboratories), diethanolamine (99%, Fluka), titaniumtetrachloride (99.9%, Aldrich), butan-2-ol (99%, AnalaR), sulfur (99%, Daejung), cadmium acetate (98%, Acros organics), sodium sulfide (64%, AnalR Normapur), lead acetate (99.5–100.5%. Research lab fine industries), zinc acetate (98.4%, Acros organic), potassium chloride (99%, BDH laboratories), methanol (100%, AnalR Normapur), 3-mercaptoproponic acid (99%, Himedia) and triton × 100 (98–102%, BDH laboratories) were used as received without further purification. Dysol paste (DSL 18-NRT, 20 nm average particle size) was purchased from Dysol company and fluorine doped tin oxide (FTO) coated glass plates were purchased from Soloronix (2.2 mm thickness, 7 $\Omega\,cm^{-2}$). All the chemicals were used without further purification as received. For the fabrication of photoanode, titanium isopropoxide solution, butan-2-ol and one drop of diethynolamine were mixed well and spin coated on top of FTO glass at 5000 rpm for one minute and dried at 130 °C for five minutes. The process of deposition was repeated three times and finally sintered at 500 °C for 40 min. Two scotch tape thickness of active layer with dysol 18NR-T transparent paste was coated on top of the blocking layer by doctor blade method followed by another layer of TiO_2 paste prepared by Pichini based sol-gel preparation method [16].

The TiO_2 paste prepared by Pichini method was synthesized as follows: ethylene glycol (1.334 ml) was heated to 60 °C and titanium isopropoxide (0.305 ml) and citric acid (1.2672 g) were added and followed by heating at 90 °C for 15 min. Once the sol became clear it was allowed to cool to room temperature and ground by mixing 0.559 g of P25 Degussa TiO_2 powder for one hour. (Titanium isopropoxide: citric acid: ethylene glycol was used in 1:6:24 ratio and titanium isopropoxide: TiO_2 in 1:7 ratio). The resulting paste was coated on top of the semi-transparent film of FTO by doctor blade method with two scotch tape thickness, and sintered at 450 °C by slow heating (ramping of temperature was 3 °C/min). Secondly, same procedure was repeated with the titanium sol prepared with the ratio of titanium isopropoxide: citric acid: ethylene glycol 1:5:20. Finally, film was treated with 40 mM $TiCl_4$ solution at 70 °C for 30 min.

PbS and CdS q-dots were deposited on TiO_2 mesoporous layer by SILAR method to fabricate the q-dot loaded TiO_2 photoanode. Aqueous solutions of 0.02 M lead acetate and 0.02 M sodium sulfide precursor solutions were used to deposit PbS quantum dot while 0.05 M cadmium acetate and 0.05 M sodium sulfide solutions were used to deposit CdS. One cycle deposition consists of immersion of the photoanode into the cationic precursor solution and followed by deposition of sulfide by immersing into the sulfide precursor solution. The sulfide precursor solutions consists 3-mercaptoproponic acid. In each deposition, the photoanode was immersed into the 3-mercaptoproponic acid mixed sulfide solution and followed the various number of PbS and CdS deposition cycles. Finally, ZnS over layer was deposited by using 0.05 M zinc acetate and 0.05 M sodium sulfide solutions. The Cu_2S counter electrode which was prepared by cleaning a piece of brass by treating with conc. HCl at 80 °C for 20 min and followed by addition of polysulfide electrolyte into the unmasked area of brass plate was used as a counter electrode. A mixture of 2 M Na_2S, 2 M S, 0.2 M KCl in methanol: water is in 7:3 (v/v) ratio was used as an electrolyte. The counter electrode with a parafilm spacer was placed on q-dot loaded TiO_2 anode filled with electrolyte for IV measurements. The active area of the cell was 0.159 cm^2.

2.2. Characterization

The cells were illuminated using a solar simulator at AM1.5G (Newport AAA solar simulator at 100 mW/cm^2). The intensity of solar cell was calibrated with standard Si-reference cell. External quantum efficiency (EQE) was measured as the function of wavelength from 300 nm to 1100 nm using Bentham PVE300 unit with a TMc300 monochromator based IPCE with the Xenon arc lamp. A calibrated type DH Si photodetector used as a reference. Scanning electron microscope image was took by Carl zeiss EVO LS 15 scanning electron microscope. Electrochemical impedance spectroscopic (EIS) measurements were performed under dark and light conditions by using Zahner Zannium universal electrochemical work station equipped with a frequency response analyzer (Thalas) in the frequency range from 0.1 Hz to 1 MHz and 10 mV amplitude ac signal. Absorbance spectra were recorded by using Shimadzu 2450 UV–Visible spectrometer. Open circuit voltage decay measurement was performed with Tektronix 3032B digital phosphor oscilloscope. Once the stable voltage reached under illumination, shutter was turn off and voltage decay was recorded.

3. Results and discussion

In this work, a layer of PbS was anchored on TiO_2 and CdS layers were deposited stepwise on PbS and the solar cell performance was investigated with respect to PbS and CdS layer thicknesses and their surface passivation properties were investigated. Cross section SEM image and EDX analysis of TiO_2/1PbS/3CdS/2ZnS photoanode is shown in Fig. S1 and the surface SEM images of TiO_2/1PbS, TiO_2/3CdS, TiO_2/1PbS/3CdS/2ZnS, and higher magnification of TiO_2/1PbS/3CdS/2ZnS are shown in Fig. S2a–d respectively. Previous work carried out on PbS/CdS type of quantum dots with the ethanedithiol treatment reported 4.65% efficiency with aqueous polysulfide electrolyte [9]. In this investigation, TiO_2 photoanode was pre-adsorbed in 3-mercaptopropionic acid-sodium sulfide precursor solution and the pre-adsorption step facilitates deposition of more quantum dots and good connection between TiO_2 and quantum dots, resulting in enhance solar cell performance. Fig. 1 shows the *I–V* characteristics of solar cells fabricated with PbS/CdS photoanode with the variation of number of PbS and CdS cycles and the measured solar cell performances are given in Table 1. The solar cell performance of the optimized structure were repeated for four times and the measured solar cell performances are given in Table S3.

As shown in Fig. 1a–c, and Table 1, for quantum dot solar cells fabricated with PbS alone, the observed Jsc are 10.1, 15.2 and 11.1 mA cm^{-2} for 1, 2 and 3 PbS cycles respectively. When the number of PbS cycles increases from 1 to 2, enhance in Jsc is noted which could be assigned to the enhance light harvesting properties of PbS. However, further increase in the number of PbS cycles resulted in decrease in Jsc which could be due to enhanced charge recombination due to formation of aggregates and bigger PbS particles [17]. Similarly, by increasing the number of CdS cycles, Jsc of 1.5, 2.2 and 2.7 mA cm^{-2} were observed for 1, 2 and 3 CdS cycles respectively. Interestingly, an average Voc of ~300 mV and FF of ~35% were observed for PbS sensitized solar cells while for

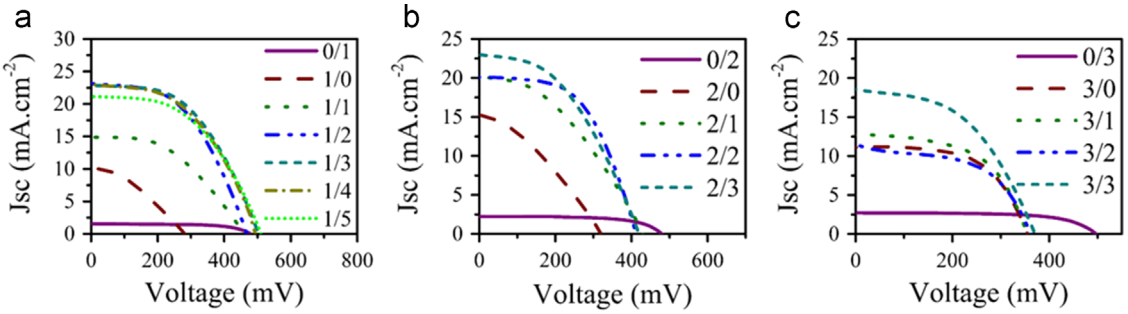

Fig. 1. Solar cell performance of (a) 1 cycle of PbS, with the variation of number of CdS cycles, (b) 2 cycles of PbS, with the variation of number of CdS cycles and (c) 3 cycles of PbS, with the variation of number of CdS cycles.

Table 1
Cell performance with various number of deposition cycles.

Cell[a] PbS/CdS	Jsc (mA cm^{-2})	Voc (mV)	FF (%)	Efficiency (%)
1/0	10.1	279.5	35.4	1.0
0/1	1.5	480.4	64.4	0.5
1/1	14.8	459.7	45.9	3.1
1/2	23.1	466.3	49.7	5.4
1/3	22.8	500.7	50.2	5.7
2/0	15.2	317.0	34.0	1.6
0/2	2.2	482.1	63.4	0.7
2/1	20.0	423.8	40.5	3.6
2/2	20.8	414.0	54.2	4.5
2/3	22.9	420.7	43.9	4.2
3/0	11.1	356.9	30.0	1.2
0/3	2.7	498.2	64.4	0.9
3/1	12.7	353.1	56.1	2.5
3/2	14.5	364.0	52.5	2.8
3/3	18.5	371.4	48.3	3.3

[a] PbS/CdS sensitized solar cells; Jsc short circuit photo current density; Voc open circuit voltage; FF fill factor.

CdS solar cells, Voc of ~480 mV and FF of ~64% were observed. These results clearly indicate that though, PbS sensitized solar cells produce higher Jsc than CdS sensitized solar cells, their Voc and FF are inferior to that of CdS solar cells. Also we noted that PbS q-dot sensitized solar cells are unstable compared to CdS solar cells. These results indicate that PbS is a good light harvesting material which is suitable for q-dot sensitized solar cells despite their lower fill factor, lower Voc values and poor stability. Major reasons for inferior FF and Voc of PbS sensitized q-dot solar cells could be due to presence of high defects states at the surface of q-dot PbS particles causing enhanced charge trapping leading to higher charge recombination [18,19]. It has been further demonstrated that the higher charge recombination in q-dot PbS particles as the main reason for its low Voc by EIS analysis together with ß-recombination model [19,20]. Enhanced solar cell performance has been reported for the core-shell PbS/CdS quantum dot solar cell and the observed higher efficiency was attributed mainly to enhanced stability and co-sensitization effect [7,8,14,17,19]. In this investigation, we noted that the observed Jsc of PbS/CdS q-dot solar cell is not the arithmetic addition of Jsc of individual PbS and CdS. As shown in Fig. 1a–c and Table 1, quantum dot solar cells fabricated with PbS/CdS exhibit higher Jsc than the individual PbS or CdS quantum dot solar cells and the observed Jsc of PbS/CdS quantum dot solar cells is higher than the adducts Jsc of both PbS and CdS alone. i.e quantum dot solar cells fabricated with one, two and three cycle of PbS deliver Jsc of 10.1, 15.2 and 11.1 mA cm^{-2} respectively while for one, two and three cycle of CdS, the observed Jsc are 1.5, 2.2 and 2.7 mA cm^{-2} respectively. However, when the number of CdS layer was increased while keeping the PbS cycle at one, i.e. 1PbS/1CdS, 1PbS/2CdS and 1PbS/3CdS, these quantum dot solar cells show remarkable Jscs of 14.8, 23.1 and 22.8 mA cm^{-2} respectively. Similar enhancement in Jsc were noted for thicker PbS layers with the increase of CdS layer thickness (Table 1) i.e. Jsc of 2PbS/1CdS, 2PbS/2CdS and 2PbS/3CdS solar cells were 20.0, 20.8 and 22.9 mA cm^{-2} respectively and Jsc of 3PbS/1CdS, 3PbS/2CdS and 3PbS/3CdS solar cells were 12.7, 14.5 and 18.5 mA cm^{-2} respectively. In all these instances, Jscs of PbS/CdS design is higher than the individual quantum dot solar cells fabricated with PbS or CdS quantum dots separately. Notably, in all these cases, the increase in Jsc with the increase in the thickness of CdS layer was observed while keeping the same layer thickness of PbS. The observed higher Jsc of PbS/CdS is not due to increase in light absorption by thicker CdS layer as evident by the light absorption spectra and external quantum efficiency (EQE) results of different solar cells fabricated with different thicknesses of PbS/CdS as explained below.

Absorption spectra of PbS, CdS and PbS/CdS with different number of cycles are shown in Fig. 2a and the corresponding EQE values of the solar cell fabricated with PbS, CdS, 1PbS/1CdS, 1PbS/2CdS and 1PbS/3CdS are shown in Fig. 2b. In the study of thickness variation of CdS, the thickness of PbS was kept at 1 SILAR cycle and 1–3 cycles of CdS were deposited on PbS by SILAR method. As shown in Fig. 2a, CdS absorbs mainly in the visible region up to 600 nm with an absorption threshold around 620 nm while PbS absorbs in the 400–800 nm region while extending its absorption to IR region (around 1200 nm which is not shown in Fig. 2a). By increasing the thickness of CdS by number of SILAR cycles in PbS/CdS structure, the increase in absorption was observed only up to 600 nm and above 600 nm the absorption remains constant indicating that the observed optical changes in the 400–600 nm regions are mainly due only to CdS. As shown in Fig. 2b, an entirely opposite EQE response was noted where the EQE response below 600 nm remain constant while the EQE response above 600 nm increases with the increase of CdS cycles in the PbS/CdS anode for the study of CdS thickness variation while keeping the thickness of PbS at 1 SILAR cycle. As the optical response above 600 nm is mainly due to PbS, the observed enhanced EQE response should come from PbS. If the optical change was considered, where the increase in optical absorption was noted only up to 600 nm due to increase in CdS amount, an increase in EQE should observe only in the 400–600 nm region but not in the 600–1200 nm region. Hence, the observed increase in Jsc with the increase in the thickness of CdS layer while keeping the PbS layer thickness the same, cannot be attributed to increase in light absorption by thicker CdS layer as evident by the light absorption spectra and EQE results. These results strongly suggest that the Jsc of PbS/CdS q-dot solar cells can be increased by varying the thickness of the CdS layer on a same thick PbS layer. Hence, it can be suggested that the enhance in Jsc of PbS/CdS solar cell after coating of CdS on PbS is not due to light harvesting effect. The different role played by the CdS layer in PbS/CdS design could be that it can function as a passivation layer in minimizing the surface defects in PbS q-dots.

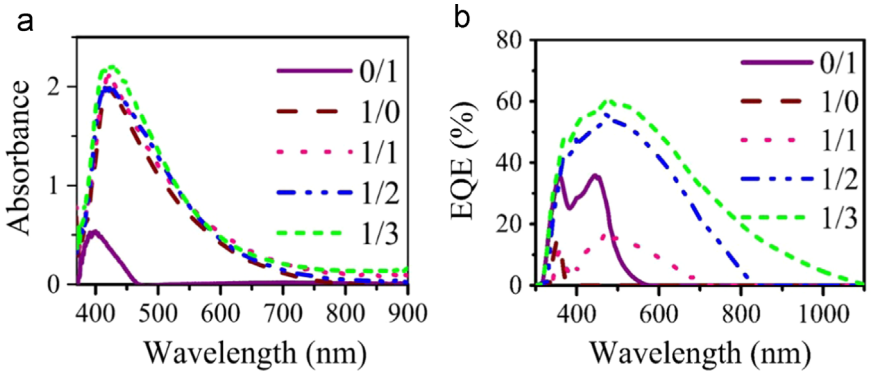

Fig. 2. (a) Absorption spectra of 1CdS, 1PbS, 1PbS/1CdS, 1PbS/2CdS and 1PbS/3CdS, (b) External quantum efficiency (EQE) spectra of 1CdS, 1PbS, 1PbS/1CdS, 1PbS/2CdS and 1PbS/3CdS.

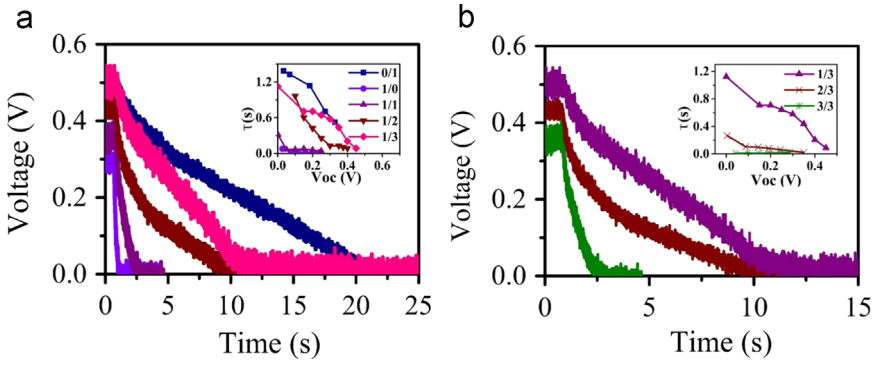

Fig. 3. (a) OCVD of 1CdS, 1PbS, 1PbS/1CdS, 1PbS/2CdS and 1PbS/3CdS and (b) OCVD spectra of 1PbS/3CdS, 2PbS/3CdS and 3PbS/3CdS. Inset in figures shows the calculated lifetime.

For the verification of surface passivation properties of CdS on PbS surface, we performed photovoltage decay measurements and electrochemical impedance spectroscopy measurements of PbS/CdS photoanode with different thicknesses of PbS and CdS.

The electron lifetime measurement of solar cells by using open circuit voltage decay (OCVD) is an interesting study to analyze recombination behavior at q-dot electrolyte interface. The OCVD spectra of 1PbS/1CdS, 1PbS/2CdS and 1PbS/3CdS are shown in Fig. 3a while OCVD spectra of 1PbS/3CdS, 2PbS/3CdS and 3PbS/3CdS shown in Fig. 3b. From the OCVD measurements, the lifetimes of electrons were calculated by using the Eq. (1) [20].

$$\tau = -(K_B T/q)(\mathrm{dVoc}/\mathrm{d}t)^{-1} \quad (1)$$

where K_B is the Boltzmann constant (1.38×10^{-23} J K^{-1}), T is the temperature, q is the elementary charge (1.69×10^{-19} C) and dVoc/dt is the derivative of the open circuit voltage transient.

For PbS electrode, a rapid photovoltage decay is noted compared to CdS electrode. When a CdS layer is coated on PbS layer, a notable slower voltage decay was observed and the voltage decay further slowed down with the increase of the thickness of the CdS layer. The lifetime values obtained from Fig. 3 using Eq. (1) are shown in the inset in Fig. 3 and the estimated lifetimes of PbS, CdS, 1PbS/1CdS, 1PbS/2CdS and 1PbS/3CdS were 0.02, 0.8, 0.08, 0.26, and 0.64 s at 0.25 V, respectively. It can be clearly observed that the lifetime of the quantum dot based on PbS is extremely low and the lifetime of PbS/CdS cells increase with the increases of number of CdS cycles. The slow voltage decay and enhanced lifetime of CdS coated PbS electrodes suggested that the coating of CdS on PbS surface causing the removal of the surface trap states and hence reduction in electron–hole recombination in PbS electrode. Interestingly, as shown in Fig. 3b, when the number of PbS cycles increases while keeping the CdS thickness at constant value, the lifetime of PbS/CdS photoanode decrease with the increase of PbS cycle which may be due to inferior surface passivation due to lack of CdS for effective passivation of thick PbS surface. Due to insufficient surface passivation, the recombination of 3PbS/3CdS is higher than that of 1PbS/3CdS which is good agreement with IV and IPCE results. Hence, the photovoltage decay results confirmed the role of CdS in passivation of PbS surfaces and a thin layer of PbS with minimized trap state density with an optimized larger number of CdS cycles showed a better solar cell performance of PbS/CdS quantum dot solar cell.

Additionally we performed EIS measurements to investigate the influence of CdS coating on the charge carrier dynamics of the PbS/CdS quantum dot photoanodes as EIS is a powerful tool to clarify the charge transfer processes at the semiconductor interface and transport resistance in quantum dot sensitized solar cell. Fig. 4 shows the Nyquist plots of the quantum dot cells fabricated with PbS, CdS, 1PbS/1CdS, 1PbS/2CdS, 1PbS/3CdS electrodes bias at Voc under illumination. In EIS spectrum, the semicircle in high frequency region represents the charge transfer resistance (Rc) Helmholtz capacitance (Cc) at the electrolyte-counter-electrode interface in parallel combination, the second semicircles are assigned to electron transport resistant in photoanode (Rt) and recombination resistance (Rk) at the interface between the PbS/CdS and electrolyte and chemical capacitance of the photoanode (Cμ). The third semicircle observed in the low frequency region corresponds to the characteristics of diffusion of the redox electrolytes electron. However, in our studies we observed only two semicircles. Also for clarity, we have shown the magnified image at high frequency region (inset in Fig. 4d).

The electrochemical impedance spectroscopy analysis were performed by fitting the parameters with equivalent circuit model and Cμ, Rt, Rk, Rc and other parameters related with counter electrode and sheet resistance (Rs) were extracted. The derived

data from impedance spectrum for Rk, Rt and Cμ are summarized in Table 2. It is clear from Table 2, that the Rk values of the bare PbS is much lower than that of CdS owing to high defect sites in PbS surface and the increase in Rk is noticeable with the increase of the thickness of the CdS layer as a result of the effective passivation of the surface traps in PbS. However, Rt of PbS is less than that of CdS and the Rt value of PbS increases with the coating of CdS layer on PbS suggesting that the charge transport become more difficult due to high electron transfer resistance of CdS. Therefore the, different behavior of PbS, CdS, 1PbS/1CdS, 1PbS/2CdS, 1PbS/3CdS electrodes and hence the solar cell efficiency could be attributed to varied passivation and electron transport resistance of PbS layer by the CdS layer.

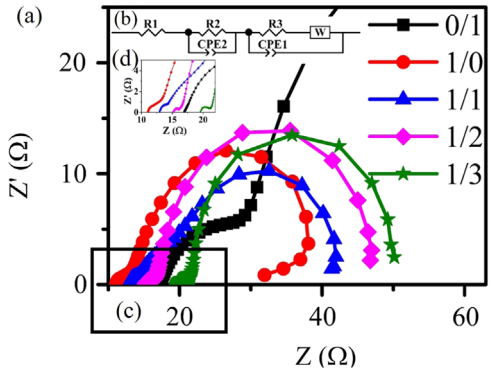

Fig. 4. (a) Nyquist plot of quantum dot solar cells (PbS, CdS, 1PbS/1CdS, 1PbS/2CdS, 1PbS/3CdS) at the open circuit bias voltage, illuminated with AM 1.5 solar light of 100 mW cm^{-2} (b) Circuit represent the q-dot solar cell (c) selected portion of graph (d) magnified image of portion (c).

Table 2
Recombination resistance (Rr), charge transfer resistance (Rt) and chemical capacitance (Cμ) of cells under one sun illumination (100 mW/cm^2). Active area of cell was kept as 0.159 cm^2 for all the measurements.

Cell PbS/CdS	Rk (Ω)	Rt (Ω)	Cμ (F cm^{-2})
1/0	24.27	0.04	0.0047
0/1	73.94	0.33	0.0855
1/1	27.75	0.09	0.0070
1/2	28.87	0.10	0.0088
1/3	29.87	0.19	0.0128

In order to give a complete explanation about the physical process inside the solar cells of PbS/CdS photoelectrode, the impedance spectroscopic analysis under dark with various bias voltage is an important tool. Fig. 5 illustrates the Cμ, Rk, σ and lifetime (τ) of PbS/CdS with the variation of PbS and CdS cycles (i.e 1PbS/1CdS, 1PbS/2CdS, 1PbS/3CdS electrodes) and (1PbS/3CdS, 2PbS/3CdS, 3PbS/3CdS electrodes) measured under dark condition. The Cμ shown in Fig. 5a is plotted against the voltage drop (V_F) in the sensitized electrode where V_F was calculated by subtracting voltage drop at the series resistance and counter electrode resistance from applied voltage [4,19].

$$V_F = V_{app} - V_{Ser} - V_{ce}. \quad (2)$$

As such, in Fig. 5a, the plot of Cμ against V_F elaborates the change of electron density as a function of Femi level and track the distributions of trap state in the band gap of semiconductor [4]. The slope of chemical capacitance vs V_F plot emphasize the density of state and the shift of chemical capacitance provide the fact about displacement of conduction band edge. From Fig. 5a, it can be observed a downward shift of the conduction band (an increase in chemical capacitance) for PbS/CdS (1PbS/1CdS, 1PbS/2CdS, 1PbS/3CdS) with the increase of CdS cycles while a slight upward shift of the conduction band is noted (a decrease in chemical capacitance) for the increase of number of PbS cycles (1PbS/3CdS, 2PbS/3CdS, 3PbS/3CdS). Hence, EIS results indicate a decrease of Voc with the increase of number of CdS layers of the PbS/CdS (1PbS/1CdS, 1PbS/2CdS, 1PbS/3CdS), while an increase of Voc is expected with the increase of number of PbS layers of the PbS/CdS (1PbS/3CdS, 2PbS/3CdS, 3PbS/3CdS). However, IV results indicated different results where an increase in Voc is noted for the PbS/CdS (1PbS/1CdS, 1PbS/2CdS, 1PbS/3CdS) system with the increase of CdS cycles

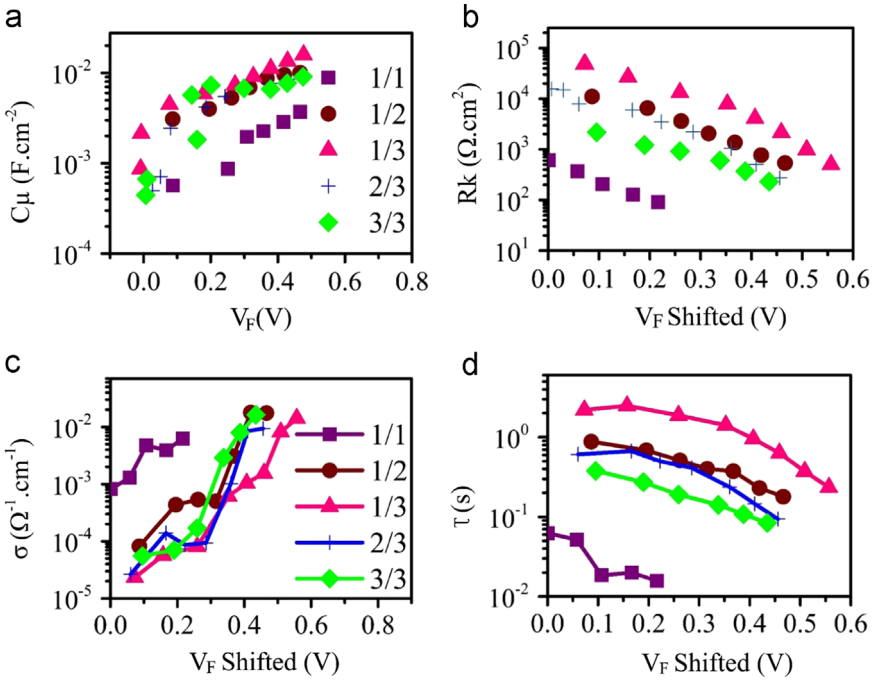

Fig. 5. (a)Chemical capacitance (Cμ) with the function of V_F (b) recombination resistance (Rk) with the function of $V_{shifted}$ (c) electron conductivity with the function of $V_{shifted}$ (d) electron life time calculated from electrochemical impedance spectroscopy with the function of $V_{F\ Shifted}$. All the parameter were derive from electrochemical impedance spectrum measured under dark condition.

while decrease in Voc noted with the PbS cycles. These results suggest that the effect of downward shift of the conduction band edge may overcome by the increase of recombination resistance with the number of CdS cycle resulting in overall increase in Voc with the increase of CdS cycles in PbS/CdS solar cells. On the other hand, the decrease in Voc with the increase of PbS cycles could be due to increase charge recombination with number of PbS cycle in PbS/CdS system (1PbS/3CdS, 2PbS/3CdS, 3PbS/3CdS) preventing accumulation of charges. Hence, the observed Voc changes with the variation of the thickness of CdS and PbS can be justified.

As it was noted the downward shift of the conduction band potential with the increase of CdS layers of PbS/CdS structure, comparison of a parameters like recombination resistance, lifetime of two cells with different conduction band potentials of TiO_2, is quite complicated due to IS parameters depend on number of electron density on TiO_2 conduction band [8,19]. Therefore, comparison of recombination resistance of different cells with various conduction band displacements does not explain the effect of recombination resistance and lifetime properly. To compare these parameters correctly with similar electron density, the conduction band position of both cells should keep as constant. In order to keep the same conduction band, the conduction band shift should be removed and graphs should plot as a function of a shifted conduction band (V_F shifted) or a common equivalent conduction band. Due to chemical capacitance is proportionally related with the conduction band shift, the plot the EIS parameters against V_F shifted permits comparison of different IS parameters with an equivalent conduction band position (i.e., the same distance between the electron Fermi level and the CB of TiO_2) which is able to elaborate the variations unambiguously [8,19].

$$C\mu = e^{-(E_{CB}-E_{F_n})/K_BT} \tag{3}$$

Fig. 5b shows the recombination resistance plotted against V_F shifted for 1PbS/1CdS, 1PbS/2CdS, 1PbS/3CdS 2PbS/3CdS and 3PbS/3CdS electrodes. The cell with 1PbS/1CdS has lower recombination resistance and the recombination resistance of these q-dots solar cells increase with the number of CdS cycles and decrease with the number of PbS cycles. The increase of number of CdS cycle leads to increase the loading of CdS quantum dots which could act as effective charge blocking layer resulting in enhanced charge recombination resistance. As a result of enhanced Rk with the number of CdS cycles, recombination of photoexcited electrons reduced and hence the Voc and Jsc of the PbS/CdS cells increase. Similarly, Rk is found to decrease with the number of PbS cycle and decreased Voc is observed for PbS/CdS solar cell with the number of PbS cycles.

Moreover, we have applied the ß-recombination model [8,19] to study the recombination properties of PbS/CdS quantum dot sensitized solar cell. In this model recombination properties of sensitized solar cell proportional to $n^{ß}$, where n and $ß$ represent electron density in TiO_2 and $ß$ parameter respectively. For an ideal device, $ß$ takes the value 1. For dye sensitized solar cells $ß$ takes values between 0.5 and 0.7 and better performing cell, $ß$ takes the value almost constant for wide range of V_F values [4]. In this $ß$-recombination model, $ß$ can be calculated from the gradient of ln Rk vs V_F graph (see supplementary information Table S2). Recombination resistance Rk related with $ß$ by

$$Rk = R_0 e^{-q\beta V_F/K_BT} \tag{4}$$

where q denote elementary charge, R_0 pre-exponential factor, K_B Boltzmann constant and T is absolute temperature. In the $ß$-recombination model, the charge transfer process could be demonstrated through distribution of surface states of TiO_2 where $ß$ value related with distribution of surface states by

$$ß = \left(\frac{1}{2}\right) + \frac{T}{T_0} \tag{5}$$

where T and T_0 are absolute temperature and exponential distribution of surface states in TiO_2 respectively [4]. In this study, despite the obtained $ß$ values for PbS/CdS photoanodes are lower than the $ß$ minimum value which is 0.5 (Table S2), $ß$ values of PbS increase with the increase of CdS loadings. These results indicate the diminish charge recombination by coating of different number of CdS q-dots SILAR cycles on PbS which could be due to variation of proper orientation of recombination path and the active passivation effect.

Electron conductivity (σ) and electron lifetime (τ_n) were calculated from impedance spectroscopy measurements by using Eq. (6) and (7) and shown in Fig. 5d and e respectively and the same voltage shift was applied to the Cμ was applied to τ_n and σ, where L and S indicate the thickness and active area of TiO_2 film.

$$\sigma = L/(Rt \cdot S) \tag{6}$$

$$\tau_n = R_{rec} \cdot C_\mu \tag{7}$$

As shown in Fig. 5c, the electron conductivity of the PbS/CdS q-dot cell decreases with number of CdS SILAR cycles while electron conductivity increase with the increase of PbS cycles. The decline trend of conductivity with the number of CdS cycles could be attributed to enhanced filling of TiO_2 pores by CdS particles at higher CdS loading preventing contact between TiO_2 particles and electrolyte [4]. Fig. 5d shows the electron life time variations with number of CdS and PbS cycles. The τ_n of the electron decrease with increasing number of PbS cycle while it increases with number of CdS SILAR cycle in PbS/CdS solar cell which was similar to OCVD results shown in Fig. 4. As both measurements gave similar results for τ_n, it is a clear evidence that the lifetime of electrons increases after coating of CdS on PbS due to suppression of charge recombination in PbS/CdS anode. However, the measurements derived from impedance spectroscopy showed higher lifetime values than the lifetime measured from OCVD methods. This difference could arise due to production of photogenerated electron–hole pairs in OCVD method in which these electron hole pairs can be trapped in surface states of QDs resulting in enhancing the charge recombination leading to lower lifetime than EIS measurement done under dark conditions.

4. Conclusion

Solar cell performance data together with EIS and OCVD data suggest that other than co-sensitization effect, CdS can acts as a passivation layer and boost the efficiency of the PbS/CdS q-dots solar cell. In PbS/CdS structure, PbS is mainly acting as light harvesting component while CdS function as a passivation layer for PbS particles. Short-circuit current of PbS/CdS solar cell can be increased with the increase of number of PbS cycles, however, an increase in charge recombination is imminent. The enhanced charge recombination of PbS can be controlled by the passivation layer of CdS. In this study, we successfully demonstrated a record performance of solar cell with Jsc of 22.8 mA cm^{-2} and an efficiency of ~5.7% for PbS/CdS sensitized quantum dot solar cell by controlling the layer thickness of CdS.

Appendix A. Supplementary material

Supplementary data associated with this article can be found in the online version at http://dx.doi.org/10.1016/j.solmat.2015.12.014.

References

[1] J.G. Radich, R. Dwyer, P.V. Kamat, Cu_2S reduced graphene oxide composite for high-efficiency quantum dot solar cells. Overcoming the redox limitations of S_2^-/Sn_2^- at the counter electrode, J. Phys. Chem. Lett. 2 (2011) 2453–2460.

[2] I. Mora-Seró, J. Bisquert, Breakthroughs in the development of semiconductor-sensitized solar cells, J. Phys. Chem. Lett. 1 (2010) 3046–3052.

[3] C. Piliego, L. Protesescu, S.Z. Bisri, M.V. Kovalenko, M.A. Loi, 5.2% efficient PbS nanocrystal Schottky solar cells, Energy Environ. Sci. 6 (2013) 3054–3059.

[4] V. González-Pedro, X. Xu, I. Mora-Sero, J. Bisquert, Modeling high-efficiency quantum dot sensitized solar cells, ACS Nano 4 (2010) 5783–5790.

[5] Z. Ning, O. Voznyy, J. Pan, S. Hoogland, V. Adinolfi, J. Xu, M. Li, A.R. Kirmani, J.-P. Sun, J. Minor, Air-stable n-type colloidal quantum dot solids, Nat. Mater. 13 (2014) 822–828.

[6] Y.C. Choi, D.U. Lee, J.H. Noh, E.K. Kim, S.I. Seok, Highly improved Sb_2S_3 sensitized-inorganic–organic heterojunction solar cells and quantification of traps by deep-level transient spectroscopy, Adv. Funct. Mater. (2014) 3587–3592.

[7] M.A. Hossain, Z.Y. Koh, Q. Wang, PbS/CdS-sensitized mesoscopic SnO2 solar cells for enhanced infrared light harnessing, Phys. Chem. Chem. Phys. 14 (2012) 7367–7374.

[8] V. Gonzalez-Pedro, C. Sima, G. Marzari, P.P. Boix, S. Gimenez, Q. Shen, T. Dittrich, I. Mora-Sero, High performance PbS Quantum Dot Sensitized Solar Cells exceeding 4% efficiency: the role of metal precursors in the electron injection and charge separation, Phys. Chem. Chem. Phys. 15 (2013) 13835–13843.

[9] M.S. de la Fuente, R.S. Sánchez, V. González-Pedro, P.P. Boix, S.G. Mhaisalkar, M.E. Rincón, J. Bisquert, I. Mora-Seró, Effect of organic and inorganic passivation in quantum-dot-sensitized solar cells, J. Phys. Chem. Lett. 4 (2013) 1519–1525.

[10] R. Ihly, J. Tolentino, Y. Liu, M. Gibbs, M. Law, The photothermal stability of PbS quantum dot solids, ACS Nano 5 (2011) 8175–8186.

[11] H. McDaniel, N. Fuke, N.S. Makarov, J.M. Pietryga, V.I. Klimov, An integrated approach to realizing high-performance liquid-junction quantum dot sensitized solar cells, Nat. Commun. 4 (2013) 2887–2896.

[12] J.W. Lee, D.Y. Son, T.K. Ahn, H.W. Shin, I.Y. Kim, S.J. Hwang, M.J. Ko, S. Sul, H. Han, N.G. Park, Quantum-dot-sensitized solar cell with unprecedentedly high photocurrent, Sci. Rep. 3 (2013) 1050–1057.

[13] L.H. Lai, L. Protesescu, M.V. Kovalenko, M.A. Loi, Sensitized solar cells with colloidal PbS-CdS core-shell quantum dots, Phys. Chem. Chem. Phys. 16 (2014) 736–742.

[14] M.A. Abbas, M.A. Basit, T.J. Park, J.H. Bang, Enhanced performance of PbS-sensitized solar cells via controlled successive ionic-layer adsorption and reaction, Phys. Chem. Chem. Phys. 17 (2015) 9752–9760.

[15] H.M. Choi, I.A. Ji, J.H. Bang, Metal selenides as a new class of electrocatalysts for quantum dot-sensitized solar cells: a tale of Cu1. 8Se and PbSe, ACS Appl. Mater. Interfaces 6 (2014) 2335–2343.

[16] U. Opara Krašovec, M. Berginc, M. Hočevar, M. Topič, Unique TiO_2 paste for high efficiency dye-sensitized solar cells, Sol. Energy Mater. Sol. Cells 93 (2009) 379–381.

[17] N. Zhou, G. Chen, X. Zhang, L. Cheng, Y. Luo, D. Li, Q. Meng, Highly efficient PbS/CdS co-sensitized solar cells based on photoanodes with hierarchical pore distribution, Electrochem. Commun. 20 (2012) 97–100.

[18] S.D. Sung, I. Lim, P. Kang, C. Lee, W.I. Lee, Design and development of highly efficient PbS quantum dot-sensitized solar cells working in an aqueous polysulfide electrolyte, Chem. Commun. 49 (2013) 6054–6056.

[19] A. Braga, S. Giménez, I. Concina, A. Vomiero, I. Mora-Seró, Panchromatic sensitized solar cells based on metal sulfide quantum dots grown directly on nanostructured TiO2 electrodes, J. Phy. Chem. Lett. 2 (2011) 454–460.

[20] S.W. Jung, J.H. Kim, H. Kim, C.J. Choi, K.S. Ahn, ZnS overlayer on in situ chemical bath deposited CdS quantum dot-assembled TiO_2 films for quantum dot-sensitized solar cells, Curr. Appl. Phys. 12 (2012) 1459–1464.